Failure stress of a disordered three-dimensional spring network

Chung, J.W; de Hosson, J.T.M.; van der Giessen, E.

Published in:
Physical Review B

DOI:
10.1103/PhysRevB.64.064202

Publication date:
2001

Failure stress of a disordered three-dimensional spring network

J. W. Chung, J. Th. M. De Hosson,* and E. van der Giessen
Department of Applied Physics, Materials Science Centre and Netherlands Institute of Metals Research, University of Groningen, Nijenborgh 4, 9747 AG Groningen, The Netherlands
(Received 7 November 2000; published 13 July 2001)

This paper concentrates on the failure stress of a disordered three-dimensional spring network. In particular, we investigate the effects of several fracture criteria and of the connectivity at the nodes in the network. A node cannot be connected with another node if its relative distance is larger than a certain cutoff radius or a so-called connectivity threshold. In our modeling approach, the spring networks were loaded in compression and the network configuration with the lowest energy was calculated after each increment of force. Subsequently, the mechanical properties of the relaxed network structures were investigated using various fracture criteria. The largest threshold value of displacement was set to the commonly used criterion for brittle fracture, i.e., a fraction criterion of 1%, but also lower values (0.75%, 0.50%, and 0.25%) were examined. In addition, for each of these fracture criteria the stress calculations were repeated with different connectivity thresholds. From this investigation it is concluded that it is not sufficient to examine only the fracture strain. In particular, the connectivity, i.e., the connectivity threshold C_0, which controls the spring entanglement between the nodes, has a substantial effect on the crack morphology. Larger C_0's result in smaller fragments caused by crack branching.

DOI: 10.1103/PhysRevB.64.064202 PACS number(s): 46.50.+a

I. INTRODUCTION

Elastic networks of springs or beams are frequently used to model the relation between mechanical properties of materials and their microstructure. An overview has been presented by Chakrabarti and Benguigui.[1] Simulations have been carried out either in three[2–9] or two[3,10,11,4] dimensions. However, mainly regular spring networks were examined. Although from these studies new concepts may emerge, a relevant question is whether these results can be transferred to experimental observations of the failure of highly porous ceramic materials. Generally speaking, these materials have a highly disordered structure and therefore this work focuses on the failure stress of a disordered three-dimensional (3D) spring network. In particular, the effects of several fracture criteria and of the connectivity of springs by varying the connectivity threshold, C_0, are investigated. The C_0 is only used to build the initial unstrained spring network from the node configurations as calculated in the dynamics step. During the rest of the loading under compression, no new bonds or interactions will be formed.

The molecular-dynamics algorithm proves to be an easy method to be employed as a generation method of node configurations, especially when average properties of the generated configuration must be random on the sample scale and need to be structured on a local scale in order to resemble the highly porous ceramics.[12,13]

In our model approach, it is important to realize that every step in the force increment leads to a linearly dependent displacement in the n-body interactions, $n=2,3,4$. The nonlinearity is caused by the removal of all node interactions during the calculations.

The removal of the interactions between nodes is determined if the relative interaction $\Delta_f(t) = 100|(I_0-I_t)/I_0|\%$ at time t deviates a certain percentage, where I_0 is the interaction of the starting configuration and I_t is the interaction at the lowest-energy configuration in step t. In the case of a two-body, the interaction denotes a bond length, and in the case of bending and torsion, the interaction denotes a bending and a torsion angle, respectively. The fracture criterion is the fracture strain, i.e., the maximum strain the material can support before failure. Bonds are removed whenever a bond meets the criterion of failure strain.

Despite the fact that the loading condition remains in compression, this does not necessarily mean that bending is the principal mode of failure. Whether the bond fails in bending or torsion strain is determined by the local structure and the geometry of its surrounding structures. Another important quantity is how the smallest cross-sectional area, which transmits the external load through the material, will be lowered during the fracturing process.

Before the compression process starts, the configuration of spheres from the dynamics calculations is converted into a configuration of nodes. The middle point of each sphere becomes the position of a node. Whether there exists an interaction or a so-called bond between two nodes in the initial configuration is determined by the cutoff radius or so-called connectivity threshold. From our description, a node cannot form a bond with another node if its relative distance is larger than a so-called connectivity threshold, C_0. Consequently, there is only bonding if the nodes in the initial configuration fulfill $I_0<C_0$. In contrast to the more frequently used Delaunay and its dual Voronoi[14] representations, the struts do not resemble a grain-to-grain contact surface. In a Delaunay representation, the number of nodes coincides with the number of grains or cells, and in our method that is not necessarily the case. In the following, the spring networks are loaded in compression, and after each force increment, the network configuration with the lowest energy is calculated. Every bond in the network configuration that meets the failure strain will be moved. As long as the top part of the sample is still connected to the bottom by bonds, the result-

ing configuration serves as the starting configuration for the next compression step. The lowest compression force at which the sample fractures is called the failure stress. The whole process is repeated with different connectivity thresholds.

II. COMPUTATIONAL PROCEDURE

The computational procedure of our method starts with the generation method of a node distribution.[2] The molecular-dynamics-based generation algorithm uses 1000 void volume spheres, which all have a Lennard-Jones[15] interacting outer surface characterized by the strength of the Lennard-Jones interaction, ε. The method provides a convenient way of generating a disordered distribution of nodes. The disorder is controlled by the preset temperature and pressure values of a thermostat.[16] The radii of the void volume spheres were taken to be 25 nm and the Lennard-Jones, σ_{LJ}, of the outer surface interaction was also set to 25 nm. The Lennard-Jones σ_{LJ} is the position of the minimum in the potential well. The temperature of the reference bath is set to be $8.0\varepsilon/k_B$ (0.78 is the Lennard-Jones triple point temperature) and the pressure reference bath has a preset value of 0.4 (1.275 is the Lennard-Jones triple point pressure). Those values were found to be sufficient to generate a disordered spatial distribution of particles.[15]

The disordering relaxation process took 20 000 time steps in order to attain equilibrium with a time increment Δt of 10^{-9} s. The leap-frog integration scheme[17] calculates the position and velocities of the particle using the Newtonian equations of motions. The driving force for each particle in each step is the superposition of all the interactions of the particle with its interacting neighboring particles. After the first 20 000 time steps, four node distributions are sampled, i.e., all the distributions were taken with 5000 consecutive time steps in between. The average of the subsequently sampled configurations will be a good representation of the equilibrated disordered system. The anisotropic pressure thermostat maintains at a constant pressure in the system by altering the box size isotropic.

The whole configuration generation process using a molecular-dynamics (MD) algorithm with 1000 void volume spheres took almost 3 h on a SGI, Power Indigo.

To eliminate the effect due to the node density itself, all the distributions were scaled to a 0.5 node density. This is the same density as in a regular configuration of nodes.

The starting configuration has the following dimensions: basal area 1 μm$\times$1 μm and a height of 2 μm. It contains 1000 nodes, resulting with a node density of 0.5 in a density of 500 nodes per μm^3.

The generated distributions form the basis of the spring-connecting procedure. Every node is a potential point of connection and as a consequence the geometry of the network is globally fixed by the positions of the nodes. Actually, only the interaction length between the nodes is left as a parameter. The node interaction between two nodes exists only if their relative distance is below the connectivity threshold, C_0. Depending on the value of C_0, the system may develop from fully connected, i.e., every node is connected with all the other nodes, to the lower limit, where all nodes are disconnected. For the lower limit of C_0, the network resembles the Delaunay network, whereas for higher C_0 values, the network geometry will deviate more and more from it. The values for the C_0 are 245, 200, and 145 nm.

Another situation that might occur is that some nodes are connected to each other but not to the rest of the bulk. Such groups are called fragments. The number of unconnected nodes and fragments will increase with decreasing C_0. Although C_0 is larger than the diameter of a void sphere, it could still lead to very poorly connected networks. Those networks might even fail at the lowest value of an externally applied load, simply because the network is below the percolation limit. The lowest value for C_0 is not very well defined in an absolute manner, like in the regular grid-based networks.[18] In fact, the lower limit is used as one of the lowest values we could take without changing the node density of the starting network configuration too much. To achieve a nearly constant node density in a randomly distributed configuration, the lowest connectivity threshold causes a density deviation, ranging between 0.5% and 2.7%.

In the following, the spring networks are loaded in compression, and after each force increment, the network configuration with the lowest energy and the strain are calculated. The fracture criteria used throughout this work are the maximum strain of 1.0%, 0.75%, 0.50%, and 0.25%. These values were also applied as fracture criteria for bond length and angular distortion.

Once the fracture strain is satisfied in a spring element, the bond is removed from the network. Each bond that deviates more than the preset fracture criterion or so-called fracture strain will be excluded during the further course of loading. Nodes without connection (floating nodes) or groups of unconnected nodes (fragments) were also removed from the interaction matrix. As a result of the removal of floating nodes and fragments, the possible effects of these fragments on the actual failure stress are explicitly ignored. An exception is maintained for the first layer on top and the last layer at the bottom of the sample with a thickness of 10.0 nm. All connections emerging from the nodes lying within these two layers are not subjected to fracture. This is done to take into account the fragmentation effect at the contact area. Actually, these unremoved nodes will effectively transmit the load similar to the ability of the fragments to transmit the load in real experiments.

In the actual calculation of the failure stress, the total elastic energy is described by a two-body central force (CF), a three-body bond bending (BB), and a four-body torsion (T) contribution,[2]

$$U_{\mathrm{EL}} = U_{\mathrm{CF}} + U_{\mathrm{BB}} + U_T . \tag{2.1}$$

The reaction central force contribution on node i, $\Delta F_i^{\mathrm{CF}}(n+1)$, with respect to the previous force, $\Delta F_i^{\mathrm{CF}}(n)$, is given by the first derivative of the central force potential U_{CF} with respect to the node position of i, q_i, i.e.,

$$\Delta F_i^{\mathrm{CF}}(n+1) = -\left[-\frac{\partial U^{\mathrm{CF}}(n+1)}{\partial q_i} \right] = -k_{ij}^{\mathrm{CF}}[\Delta \mathbf{u}_{ij}(n+1)\cdot \hat{R}_{ij}(n)]\hat{R}_{ij}^{q}(n), \tag{2.2}$$

where the CF potential is described by

$$U^{\mathrm{CF}}(n+1) = \tfrac{1}{2}\sum_{\langle ij\rangle} k_{ij}^{\mathrm{CF}}[\Delta \mathbf{u}_{ij}(n+1)\cdot \hat{R}_{ij}(n) + |\mathbf{R}_{ij}(n)| - |\mathbf{R}_{ij}(0)|]^2. \tag{2.3}$$

The $\langle ij\rangle$ denotes the summation over all ij pairs of connected nodes. The bond vector $\mathbf{R}_{ij}(n)$ from node i to node j ($\equiv$bond ij) at increment n is defined as $\mathbf{r}_j(n)-\mathbf{r}_i(n)$, where $\mathbf{r}_j(n)$ is the position of node j at increment n. Furthermore, the displacement increment $\Delta \mathbf{u}_{ij}(n)$ at increment n is given by $\mathbf{u}_j(n)-\mathbf{u}_i(n)$, where $\Delta \mathbf{u}_i(n)\equiv \mathbf{u}_i(n+1)-\mathbf{u}_i(n)$ is the bond displacement increment of node i and $\mathbf{u}_i(n)\equiv \mathbf{r}_i(n) - \mathbf{r}_i(0)$ represents the displacement of node i at increment n. The force constant for the CF is

$$k_{ij}^{\mathrm{CF}} = \frac{A_{ij}E_{ij}}{|\mathbf{R}_{ij}(0)|}, \tag{2.4}$$

where A_{ij} is the cross-sectional area of bond ij (all cross sections are assumed to be circular) and the E_{ij} is Young's modulus. The magnitude of the force constant is inversely proportional to the initial bond length.

For the bond-bending potential (the three-body term), between nodes ijk, where i is the center of the hingelike bond-bending potential, U_{BB}, the following expression is used:

$$U_{\mathrm{BB}}(n+1) = \tfrac{1}{2}\sum_{\langle ijk\rangle} k_{ij}^{\mathrm{BB}}[\Delta\theta_{ijk}^{ij}(n+1) + \Delta\theta_{ijk}^{ik}(n+1) + \theta_{ijk}(n)]^2. \tag{2.5}$$

$\Delta\theta_{ijk}^{ij}(n+1)$ and $\Delta\theta_{ijk}^{ik}(n+1)$ are the angular deviations in step $n+1$, due to beamlike bending of the bond ij and ik. The force constant

$$k_{ijk}^{\mathrm{BB}} = \left(\frac{1}{k_{ijk}^{ij}} + \frac{1}{k_{ijk}^{ik}} \right)^{-1}, \tag{2.6}$$

where k_{ijk}^{ij} and k_{ijk}^{ik} are taken from elasticity theory of a bending beam. The first component is given by

$$k_{ijk}^{ij} = \frac{3E_{ij}I_{ij}}{|\mathbf{R}_{ij}(n)|}, \tag{2.7}$$

where I_{ij} is the second moment of area of bond ij. The second one k_{ijk}^{ik} of bond ik is found similarly.

The torsion interaction U_T along the bond ik due to the relative motions of bond ij and bond kl is a pseudo-four-body potential. When bonds ij and kl are projected on a plane perpendicular to the bond vector ik, this yields a three-body problem, $j-i-k-l \Rightarrow (j-i'-l)$ with $i'=(ik)$. The torsion potential is therefore actually a $(ik)jl$ bond-bending poten-

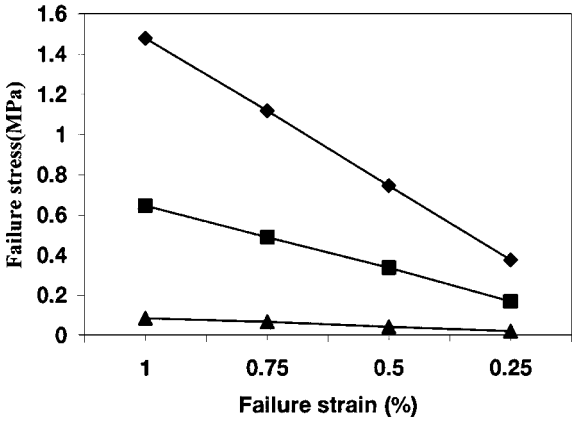

FIG. 1. Failure stress σ_F (MPa) vs the fracture strain (%) for various connectivity thresholds (▲, 145 nm; ■, 200 nm; ♦, 245 nm).

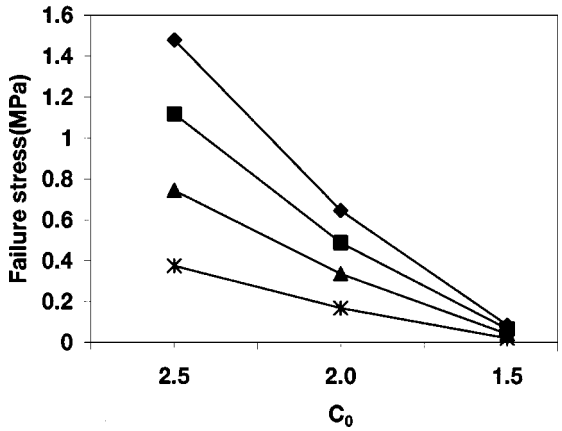

FIG. 2. Failure stress σ_F (MPa) as a function of the connectivity threshold (nm) for various fracture strains (♦, 1%; ■, 0.75%; ▲, 0.50%; ×, 0.25%).

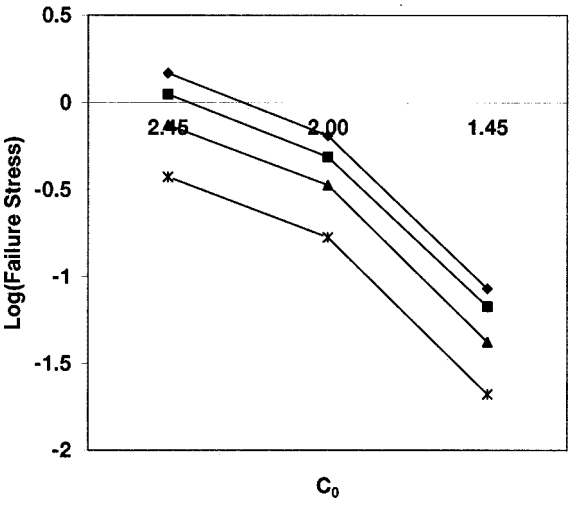

FIG. 3. Semilog plots of the failure stress σ_F (MPa) vs connectivity threshold C_0 at various fracture strain (▲, 145 nm; ■, 200 nm; ♦, 245 nm).

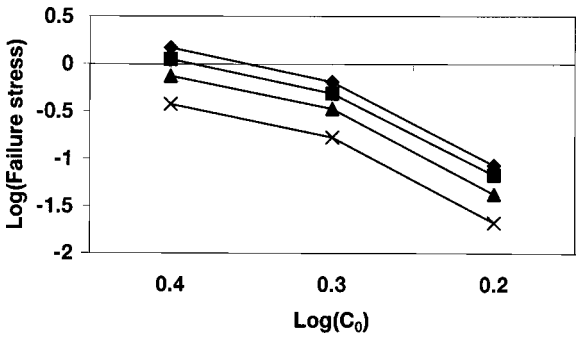

FIG. 4. Double log plot of the failure stress σ_F (MPa) vs connectivity threshold C_0 (nm) for various fracture strains (◆, 1%; ■, 0.75%; ▲, 0.5%; ×, 0.25%).

tial in the *ik* plane, where (*ik*) stands for the point in the *ik* plane where bond *ik* intersects the *ik* plane. The potential can now be written as

$$U_T(n+1)=\tfrac{1}{2}\sum_{\langle ijkl\rangle} k^T_{ijkl}[\Delta\phi_{ijkl}(n+1)+\phi_{ijkl}(n)]^2 \tag{2.8}$$

and ϕ_{ijkl} is the angle in the *ik*-plane-projected system. As for bond bending, the torsion force constant is taken from elasticity theory,

$$k^T_{ijkl}=\frac{E_{ik}I_{ik}}{(1+\nu)|\mathbf{R}_{ik}(n)|}, \tag{2.9}$$

where ν is Poisson's ratio.

When all the node-node interactions are added into the global matrix, a system of (three times the number of spheres) $3N$ linear equations is formed, or $\Delta\mathbf{F}(n+1)=[K]\Delta\mathbf{u}(n+1)$, where $\Delta\mathbf{F}(n+1)$ is a $3N$-dimensional vector of the applied force increments at compression step n, $[K]$ is the $3N\times3N$ stiffness matrix, and $\Delta\mathbf{u}(n+1)$ is the $3N$-dimensional vector of the displacement increments in the compression step *n*. The external force is applied through the force vector. This leads to the possibility of global network displacements.

The resulting displacement increments are formally found from $\Delta\mathbf{u}(n+1)=[K]^{-1}\Delta\mathbf{F}(n+1)$, but are actually obtained by solving the system of equations using a preconditioned conjugate gradient algorithm,[9] which exploits the fact that $[K]$ is a sparse matrix. Note that the $\mathbf{F}(n)$ terms do not explicitly enter this equation. The new positions at the end of increment $n+1$ are updated according to $\mathbf{r}_i(n+1)=\mathbf{r}_i(n)+\Delta\mathbf{u}_i(n+1)$.

TABLE I. Size of the final fragments of the network after fracturing, expressed in number of nodes in a fragment, at various fracture strain and connectivity thresholds.

Fracture strain (%)	Connectivity threshold C_0 (nm)		
	245	**200**	**145**
1	345	703	753
	160	184	198
	39	9	
	38	6	
0.75	159	514	722
	152	170	198
	48	17	21
	30	12	5
0.5	152	595	752
	150	150	199
	15	35	1
	10	19	
0.25	160	595	749
	148	150	215
	40	45	
	24	19	

III. RESULTS

For the computer experiments, five independent node distributions were used. This means that each node distribution was used with all the possible combinations of parameters, e.g., fracture criteria and connectivity threshold C_0. As a

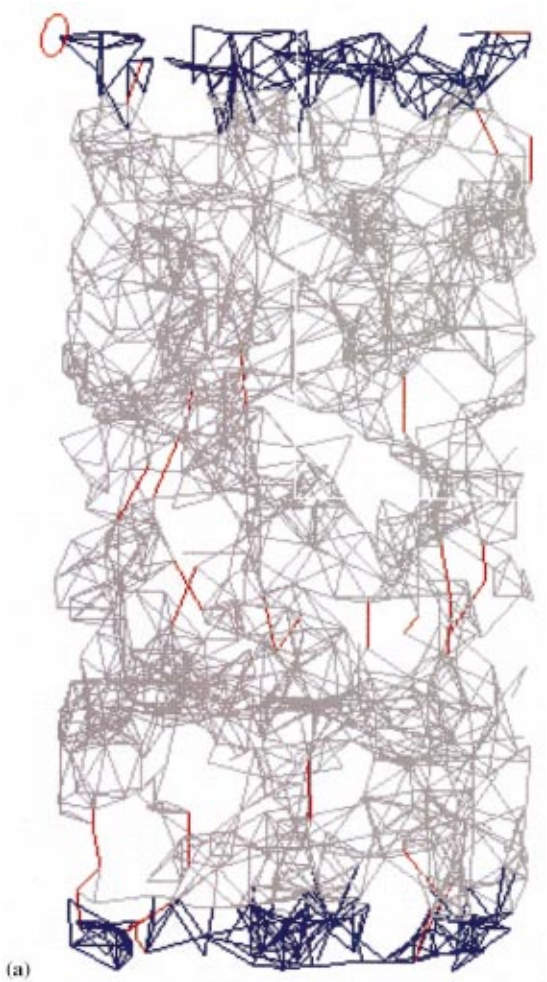

FIG. 5. (Color) Projected 3D network at three stages of deformation with a connectivity threshold of 125 nm and using a fracture criterion of 1%.

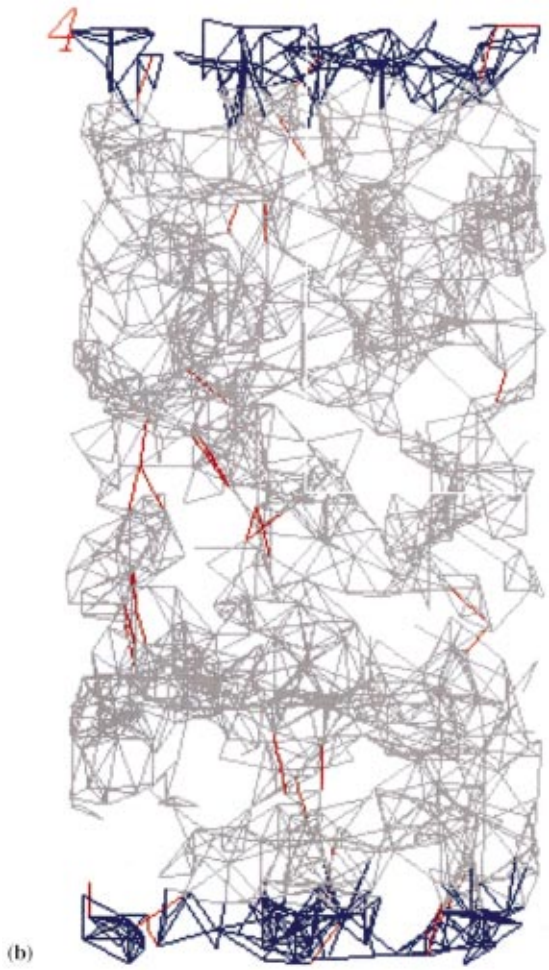

FIG. 5. (*Continued*).

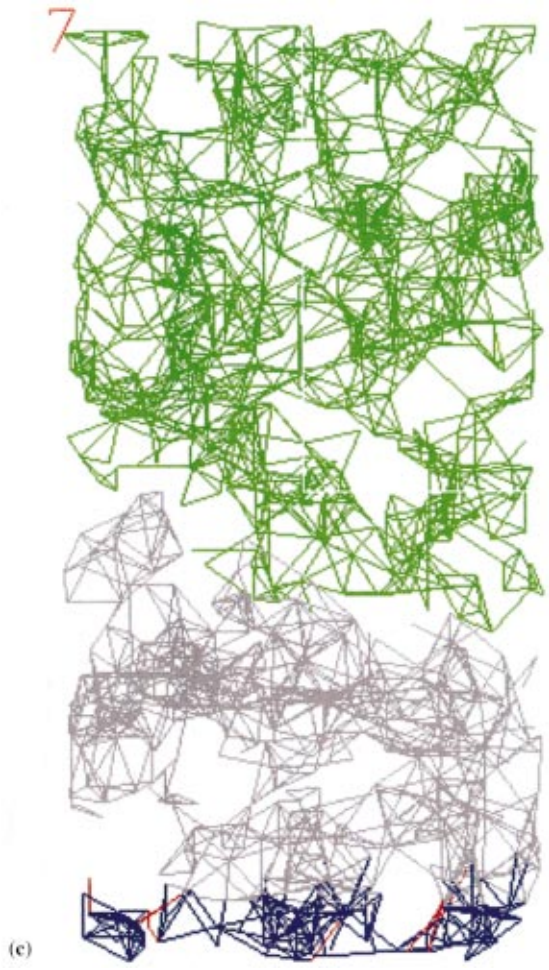

FIG. 5. (*Continued*).

consequence, the variations in failure stress due to the parameters are not caused by differences in the node distribution itself. The unit length, which is also the bond radius, is 100 nm and Young's modulus was set equal to 400 GPa. Using these material properties, the calculations led to a failure stress in the 10-MPa range, which is reasonable for highly porous ceramic materials.[2] In macroscopic porous ceramics, the failure stress, which is strongly affected by homogeneity, lies around a few MPa. The connectivity threshold fixes the average coordination number in every configuration. In this work, the C_0 values 245, 200, and 145 nm yield the average coordination numbers 12.5, 7.1, and 2.85, respectively.

A linear relationship between the failure stress and the fracture criterion is displayed in Fig. 1. It is noteworthy that this linearity does not depend on the connectivity threshold itself. From the failure stress versus the connectivity threshold (Fig. 2), we can conclude that the failure stress seems to converge towards a limit at a lower connectivity threshold. The failure stress scales approximately with the fracture criterion. This is not an exponential behavior because the semilog plot of the failure stress versus the failure strain for various connectivity thresholds is nonlinear (Fig. 3). A double log plot (Fig. 4) shows that the failure stress does not depend on the connectivity threshold in a power-law manner. All the deviations in the failure stress at various connectivity thresholds due to the differences in fracture criteria seem to be diminishing with decreasing C_0. The lower bound displayed in Fig. 2 is not fully reachable, while maintaining a nearly constant node density in all the spring networks.

By successive removal of bonds, the method shows a progressive failure that is characterized by the sizes of the fragments left behind. The average sizes of the fragments are listed in Table I. It indicates that the size of the fragments does not depend on the fracture criteria at small C_0. However, significant effects are observed if the connectivity threshold is enlarged. While the fracture criteria are of no influence on the sizes of the fragments for a connectivity threshold of 145 nm, the size of the fragments decreases upon decreasing the fracture strain at a connectivity threshold of 245 nm. At a constant fracture strain, the size of the fragments decreases with increasing connectivity threshold C_0.

The external force is applied directly through the force vector and subsequently the displacements are derived (see Sec. II). By doing so, the resulting failure stress is an upper bound of the stress in a stress versus displacement curve. In this way, no information about the behavior of the networks

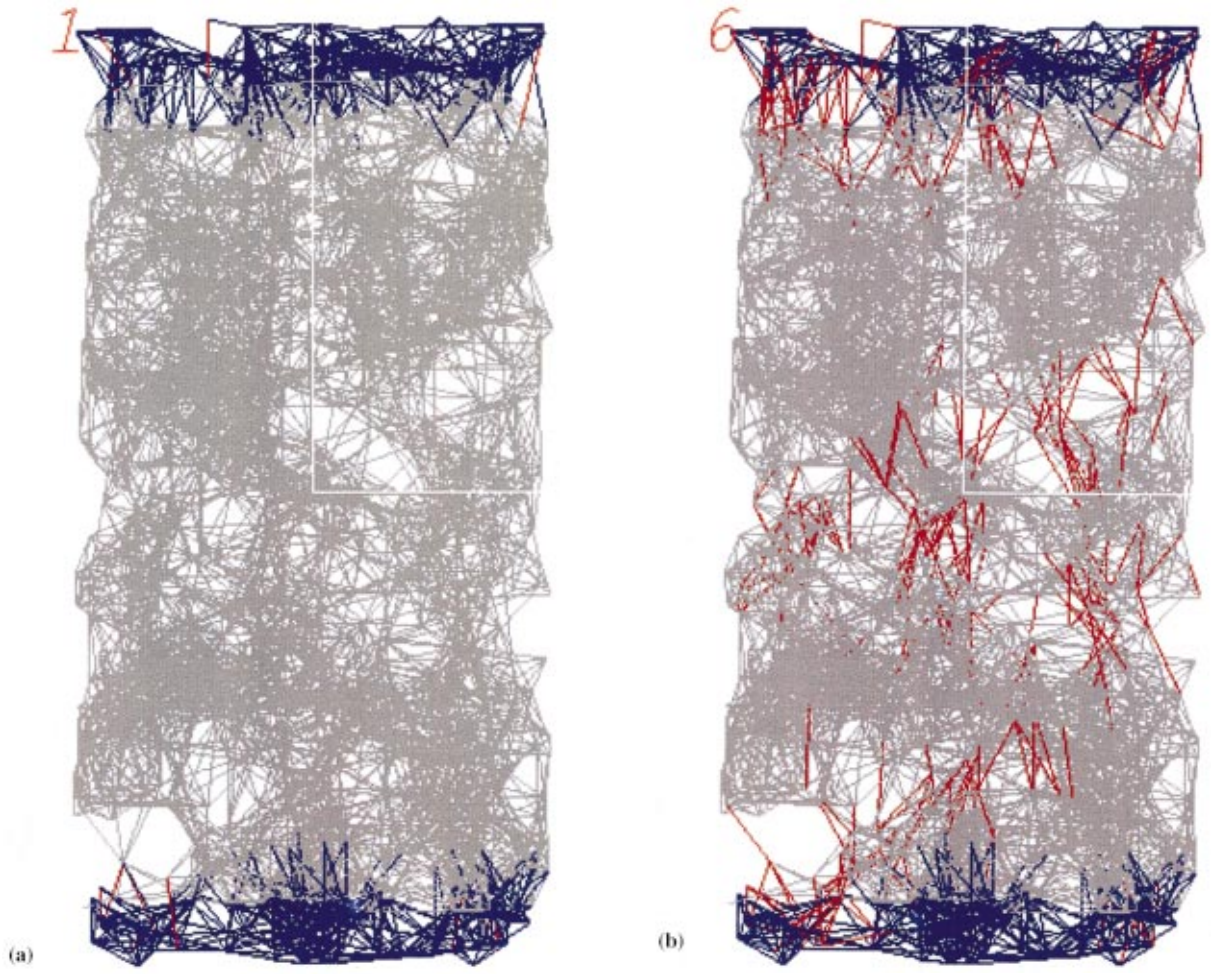

FIG. 6. (Color) Projected 3D network at three stages of deformation with a connectivity threshold of 200 nm and using a fracture criterion of 1%.

beyond the maximum stress is modeled. The fracture process can be followed in Figs. 5(a)–5(c) for a connectivity threshold equal to 145 nm, and in Figs. 6(a)–6(c) for the case of a connectivity threshold of 200 nm. The suffix "*a*" refers to the onset of the fracture process, whereas "*b*" is in between and "*c*" is after the fracture process. The color codes in Figs. 5 and 6 are the same. Blue means that the spring is attached to a node in the compression layer on the top or bottom of the sample. If a spring is colored red, the it means that it fulfills the fracture criteria. Finally, in the *c* series (Figs. 5 and 6) green is used to distinguish the upper part from the lower part of the sample after the fracture procedure.

IV. DISCUSSION AND CONCLUSIONS

In contrast to what is commonly accepted, the fracture process of 3D disordered brittle networks cannot be modeled by simply tuning the fracture strain of the disordered network. Actually, one needs to tune the combination of two network properties, that is to say, both the fracture strain and the connectivity threshold, i.e., details about the connectivity.

As illustrated in Fig. 1, the failure stress depends linearly on the fracture strain while Table I indicates an appreciable dependence of the size of the fragments on the fracture strain for larger values of C_0. Although the force and consequently also the stress are defined linearly against the displacement, the crack morphology is quite different when varying the fracture strain at various connectivity thresholds.

By the removal of fragments, the external stress will be transmitted over a smaller cross section than in the case in which the fragments remain in the sample. In addition to the not fully fractured sample, the leftovers may still transmit the load. By doing so, the debris causes a decrease in the local stress. In contrast, in this study the fragments are removed and therefore the failure stress is always a lower bound in comparison with a real experiment.

The crack morphology itself is not affected by the fracture strain for small connectivity thresholds. Despite the linear relationship between the failure stress and the fracture strain for all values of the connectivity thresholds, the crack morphology is quite different at larger values for C_0 values. At low values of the connectivity threshold, the network topology resembles a Delaunay-like topology. Consequently, the exact fracture criteria are of no importance for networks of regularly shaped grains or cells at equal distances. At larger values of C_0, the network topology is more comparable with irregularly shaped grains/cells. In addition, the crack mor-

FIG. 6. (*Continued*).

phology becomes more branched if the fracture strain is decreased.

Some remarks can be made about our choice to introduce the boundary conditions by means of a force vector. In principle, the external force can be applied either directly though the force vector or through the displacement fields. However, these different approaches do not necessarily lead to the same results. In the case of displacement-controlled deformation, the nodes in the compression contact area are explicitly positioned, while in the case of stress-controlled deformation, these nodes are pressed uniformly by a preset value of the applied force. In the case of the displacement-controlled method, the nodes at the boundary are constrained to remain in plane, whereas in the method with a directly applied force, the nodes are allowed to move along the compression axis as long as the compression force fulfills the boundary condition set by the applied load. In the latter, an additional constraint was introduced, namely all the bonds attached to the compression surface nodes are not subjected to failure. Most of the fracture occurred much farther away from the compression surface than in the first layer, which suggests that this additional constraint is sufficient to make our approach comparable to the more commonly used method based on a displacement field.

In the 3D disordered networks investigated, the effects of the connectivity threshold are clearly visible. The connectivity threshold, which controls the spring entanglement between the nodes, has a substantial effect on the crack morphology. Larger connectivity thresholds result in smaller fragments caused by crack branching.

Finally, the networks of the type considered here, with central force as well as bending and torsion interactions between nodes, can also be treated with other methods. In particular, such networks are similar to what are termed ''frameworks'' in structural engineering.[11] The networks considered here can also be analyzed by computational structural mechanics techniques, especially finite-element methods.[19,20] The important difference from the present approach from a computational point of view is that these finite-element methods involve a more efficient method to incorporate bending and torsion, but the number of degrees of freedom in a given network is twice as large as in the present approach, where one has to solve three equations for each node.[21,22]

ACKNOWLEDGMENTS

The work described in this paper is part of the research program of the Foundation for Fundamental Research on Matter (FOM Utrecht) and has been supported by the Netherlands Organization for Scientific Research (NWO–The Hague). The authors are grateful to Arjen Roos for discussions, Dr. E. Botta and Dr. A. Van der Ploeg for providing us the matrix solver, and J. Kraak (HPC computing Center, University of Groningen) for assistance in the computer visualization part.

*Corresponding author. Email address: hossonj@phys.rug.nl

[1] B. K. Chakrabarti and L. Gilels Benguigui, *Statistical Physics of Fracture and Breakdown in Disordered Systems* (Clarendon, Oxford, 1997).
[2] J. W. Chung, A. Roos, J. Th. M. De Hosson, and E. van der Giessen, Phys. Rev. B **54**, 15 094 (1996).
[3] I. C. van den Born, A. Santen, H. D. Hoekstra, and J. Th. M. De Hosson, Phys. Rev. B **43**, 3794 (1991); and in *Fracture Processes in Concrete, Rock and Ceramics*, edited by J. J. M. van Mier, J. G. Rots, and A. Bakker (E & FN SPON, London, 1991), p. 231.
[4] M. Sahimi and S. Arbabi, Phys. Rev. B **47**, 695 (1993).
[5] S. Arbabi and M. Sahimi, Phys. Rev. B **41**, 772 (1990).
[6] S. Arbabi and M. Sahimi, Phys. Rev. B **38**, 7173 (1988).
[7] S. Arbabi and M. Sahimi, Phys. Rev. Lett. **65**, 725 (1990).
[8] J. Wang, J. Phys. A **22**, L291 (1989).
[9] S. Arbabi and M. Sahimi, J. Phys. A **23**, 2211 (1990).
[10] S. Feng, P. N. Sen, B. I. Halperin, and C. J. Lobb, Phys. Rev. B **30**, 5386 (1984).
[11] H. J. Hermann, A. Hansen, and S. Roux, Phys. Rev. B **39**, 637 (1989).
[12] J. Aué and J. Th. M. De Hosson, Appl. Phys. Lett. **71**, 1347 (1997).
[13] J. Aué and J. Th. M. De Hosson, J. Mater. Sci. **33**, 5455 (1998).
[14] A. Gervois and D. Bideau, *Some Geometrical Properties of Two-Dimensional Hard Disk Packings*, in *Disorder and Granular*

Media, edited by D. Bideau and A. Hansen (Elsevier, Amsterdam, 1997), pp. 1–34.
[15] M. P. Allen and D. J. Tildesley, *Computer Simulations of Liquids* (Oxford University Press, Oxford, 1992).
[16] H. J. C. Berendsen, J. P. M. Postma, W. F. van Gunsteren, A. DiNola, and J. R. Haak, J. Chem. Phys. **81**, 3684 (1984).
[17] R. W. Hockney, Methods Comput. Phys. **9**, 136 (1970).
[18] D. Stauffer and A. Aharony, *Introduction to Percolation Theory*, 2nd ed. (Taylor & Francis, London, 1992).
[19] Y. Kantor and I. Webman, Phys. Rev. Lett. **52**, 1891 (1984).
[20] T. J. R. Hughes *The Finite Element Method* (Prentice-Hall, Englewood Cliffs, NJ, 1987).
[21] A. van der Ploeg, Ph.D. thesis, University of Groningen (1994).
[22] J. W. Chung and J. Th. M. De Hosson (unpublished).